Kinetic Study of the Intercalation of Cobaltocene by Layered Metal Dichalcogenides with Time-Resolved in Situ X-ray Powder Diffraction

John S. O. Evans,† Stephen J. Price, Heng-Vee Wong, and Dermot O'Hare*

Contribution from the Inorganic Chemistry Laboratory, University of Oxford, South Parks Road, Oxford, OX1 3QR, U.K.

Received June 1, 1998

Abstract: Energy-dispersive X-ray diffraction (EDXRD) has been used to perform in situ kinetic studies on the intercalation of cobaltocene, $Co(\eta\text{-}C_5H_5)_2$, into the layered dichalcogenides ZrS_2, 2H-SnS_2, 2H-$SnSe_2$, 2H-TaS_2, 2H-NbS_2, 1T-TaS_2, and TiS_2. Integrated intensities of the Bragg reflections have been used to determine the extent of reaction (α) versus time for each of these reactions. The half-lives ($t_{1/2}$) for reaction of an excess of cobaltocene with ZrS_2, 2H-SnS_2, 2H-$SnSe_2$, 2H-TaS_2, 2H-$NbSe_2$, and TiS_2 at 120 °C in dimethoxyethane were found to be <5, 31, 410, 16000, 2960, and >60000 s, respectively. A number of kinetic models have been considered, including the Avrami−Erofeyev ($m = 1.5$) deceleratory nuclei-growth model and statistical simulation. The activation energy for the intercalation of $Co(\eta\text{-}C_5H_5)_2$ in 2H-SnS_2 has been determined to be 41 kJ mol^{-1}. The concentration and solvent dependence of the rate of $Co(\eta\text{-}C_5H_5)_2$ intercalation into 2H-SnS_2 has also been determined. Surprisingly we find that the rate of intercalation is invariant to the initial $Co(\eta\text{-}C_5H_5)_2$ concentration over the whole concentration range studied.

Introduction

Some of the earliest and most extensive studies of the kinetics of intercalation reactions were carried out with graphite crystals. For example, Hooley and co-workers[1,2] investigated the weight gain of a graphite flake in a bromine atmosphere. More recently, other groups have looked at the kinetics of domain interconversion in graphite intercalation compounds (GIC's) from both an experimental[3−8] and theoretical[9−11] viewpoint. Surprisingly, much less attention has been focused on kinetic and mechanistic investigations of other intercalation systems such as transition metal chalcogenide intercalation or intercalation in clay minerals. This disparity may be attributable to the difficulty of performing structural studies on chalcogenide samples which, unlike graphite intercalation compounds, are not readily available as large oriented single crystals. Without the coherent scattering from planes of oriented crystal samples, the quality of diffraction spectra that can be obtained on time scales feasible for extracting kinetic data is usually too poor to be of any conceivable use.

Consequently, researchers turned to indirect methods such as titration,[12,13] mass gain,[14,15] electrochemical methods,[16−18] and spectroscopic methods[19−23] to obtain kinetic data on the intercalation reactions of layered metal chalcogenides. Until recently only a limited number of time-resolved diffraction studies on metal chalcogenide intercalation had been reported.[24−33]

† Current address: Department of Chemistry, University Science Laboratories, South Road, Durham, DH1 3LE.

(1) Hooley, J. G. *Carbon* **1973**, *11*, 225.
(2) Hooley, J. G. *Can. J. Chem.* **1962**, *40*, 749.
(3) Qian, X. W.; Stump, D. R.; S. A. Solin. *Phys. Rev. B* **1986**, *33*, 5756−69.
(4) Mcghie, A. R.; Milliken, J.; Fischer, J. E. *Mol. Cryst. Liq. Cryst.* **1982**, *86*, 1969.
(5) Milliken, J.; Fischer, J. E.; Mcghie, A. R. *Carbon* **1982**, *20*, 134.
(6) Kim, H. J.; Fischer, J. E. *Phys. Rev. B: Condens. Matter* **1986**, *33*, 4349−4351.
(7) Huang, Y. Y.; Stump, D. R.; Solin, S. A.; Heremans, J. *Solid State Commun.* **1987**, *61*, 469−473.
(8) Hooley, J. G. *Carbon* **1985**, *23*, 579−584.
(9) Ulloa, S. E.; Kirczenow, G. *Phys. Rev. Lett.* **1985**, *55*, 218−221.
(10) Kirczenow, G. *Synth. Met.* **1988**, *23*, 1−6.
(11) Kirczenow, G. *Phys. Rev. Lett.* **1985**, *55*, 2810−2813.
(12) Subba-Rao, G. V.; Shafer, M. W. *J. Phys. Chem.* **1975**, *79*, 557−560.
(13) Acrivos, J. V.; Dellos, C.; Topsoe, N. Y.; Salem, J. R. *J. Phys. Chem.* **1975**, *79*, 3003−10.
(14) Kikkawa, S. *J. Solid State Chem.* **1980**, *31*, 249−255.
(15) Dines, M. B. *Science* **1975**, *188*, 1210.
(16) Bruce, P. G.; Saidi, M. Y. *Solid State Ionics* **1992**, *51*, 187−190.
(17) Deroo, D.; Pedone, D.; Daland, F. *J. Appl. Electrochem.* **1990**, *20*, 835−840.
(18) Riekel, C.; Reznik, H.; Schollhorn, R. *J. Solid State Chem.* **1980**, *34*, 253−262.
(19) Butz, T.; Saitovitch, H.; Lerf, A. *Chem. Phys. Lett.* **1979**, *65*, 146−149.
(20) Butz, T.; Huebler, A. *Nuovo Cimento Soc. Ital. Fis.* **1983**, *2D*, 1971−1976.
(21) Butz, T.; Lerf, A.; Besenthal, J. O. *Rev. Chim. Miner.* **1984**, *21*, 556−587.
(22) Butz, T.; Lerf, A.; Besenhard, J. O. *Rev. Chim. Miner.* **1984**, *21*, 556−587.
(23) Ganal, P.; Butz, T.; Lerf, A. *Synth. Met.* **1989**, *34*, 641−5.
(24) Riekel, C.; Reznik, H. G.; Schollhorn, R. *J. Solid State Chem.* **1980**, *34*, 253−262.
(25) Riekel, C.; Fischer, C. O. *J. Solid State Chem.* **1979**, *29*, 181−90.
(26) Riekel, C.; Schollhorn, R. *Mater. Res. Bull.* **1976**, *11*, 369−376.
(27) Paulus, W.; Katzke, H.; Schollhorn, R. *J. Solid State Chem.* **1992**, *96*, 162−168.
(28) Chianelli, R. R.; Scanlon, J. C.; Raoj, B. M. L. *J. Electrochem. Soc.* **1978**, *125*, 1563.
(29) Levy-Clement, C. *Nato ASI Ser. B* **1987**, *172*, 447−55.
(30) Dahn, J. R.; Py, M. A.; Haering, R. R. *Can. J. Phys.* **1982**, *60*, 307.
(31) Marcus, B.; Soubeyroux, J. L.; Touzain, P. *NATO ASI Ser. B* **1987**, *172*, 375−378.
(32) Chabre, Y. *Nato ASI Ser. B* **1993**, 181−192.
(33) Ripert, M.; Pannetier, J.; Chabre, Y.; Poinsignon, C. *Mater. Res. Soc. Proc.* **1991**, *210*, 359.

10.1021/ja9819099 CCC: $15.00
Published on Web 10/09/1998

For example, in a pioneering study, Riekel and Schollhorn measured time-resolved neutron diffraction data during the intercalation of 2H-TaS_2 by NH_3(g) yielding a qualitative understanding into the intercalation process. However, the available levels of beam flux, while high by neutron standards, necessitated either very large sample sizes (~15 g) or long acquisition times, making a thorough, quantitative study under varying reaction conditions of temperature, concentration, and particle size unfeasible. Moreover, because of the large incoherent scattering from hydrogen atoms by neutrons, the samples studied had to be highly deuterated, which is an expensive and not always achievable prerequisite for other intercalation reactions. Recently, McKelvy and co-workers have demonstrated elegantly that in situ high-resolution transmission electron microscopy (HRTEM) measurements can be performed during the intercalation of NH_3 into TiS_2 and the deintercalation of Hg from Hg_xTiS_2 in specially constructed environmental cells. These studies have provided fascinating insights into these reactions at the molecular level.[34−37] Paulus et al. used in situ X-ray diffraction to study the intercalation of solvated Cs^+ ions into NbS_2 single crystals and pressed powder electrodes.[27] While the small quantities required for such experiments were a significant advance over the earlier neutron diffraction techniques, the cell design and geometry limited the application of this technique to electrochemical intercalation at moderate rates (time resolution ~30 min per diffractogram). Even taking all these previous experiments into consideration we still have a fairly rudimentary understanding of the intimate mechanism of these reactions. The critical factors which control the rates of these reactions are still based on trial and error experiments. A schematic picture that is still commonly used to illustrate these reactions is shown in Figure 1a; undoubtedly this greatly oversimplifies the true picture.

In recent years the technological and experimental advances in energy-dispersive powder diffraction with synchrotron X-ray sources have provided new possibilities for the solid-state kineticist.[38−41] The markedly higher intensity (several orders of magnitude) over conventional laboratory X-ray sources allows the acquisition of good quality spectra from milligram samples on a time scale of seconds, making kinetic studies of fast intercalation reactions a realizable goal. The energy distribution of the X-rays (5−140 keV) is such that they are not significantly attenuated by a variety of materials suitable for cell windows, facilitating the construction of sealed sample holders. Moreover, the fixed geometry of this technique greatly simplifies the design of any sample environment. The less stringent space constraints in synchrotron X-ray diffractometers also allow construction of more elaborate sample cells which can accommodate a wider variety of reactants, such as single crystal or microcrystalline hosts, reacting with solvated or gas-phase guests, all within a sealed, dry, anaerobic sample environment. We have recently reported the construction and commissioning of an environmental cell for measuring time-resolved energy-dispersive X-ray diffraction data for fast intercalation reactions of potentially air-sensitive materials.[42,43] Perhaps the most important aspect of this cell design is that it allows the recording of diffraction data of a wide variety of intercalation reactions under normal laboratory synthetic conditions.

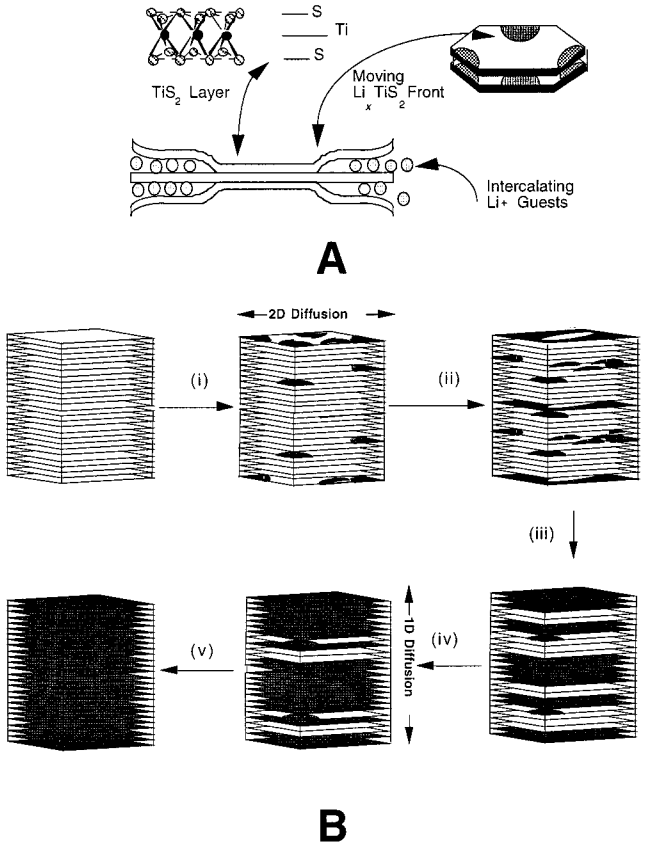

Figure 1. (a) Simple representation of the intercalation of a guest (Li^+ ions) into a layered dichalcogenide host lattice (TiS_2). (b) A more detailed breakdown of the various processes possible during intercalation as included in FIASCO2 simulations.

We report here the results of a detailed study of the rates of intercalation of the archetypal metallocene guest, cobaltocene {$Co(Cp)_2$; Cp = η-C_5H_5}, in a wide range of lamellar transition metal dichalcogenides ZrS_2, 2H-SnS_2, 2H-$SnSe_2$, 2H-TaS_2, 2H-$NbSe_2$, 1T-TaS_2, and TiS_2. The aim being to determine the rates of these reactions and hopefully gain an insight into their mechanism.

Experimental Details

Synthesis of Reactants. The syntheses of 2H-SnX_2 (X = S, Se) were based on procedures established by Al-Alamy and Balchin.[44] Stoichiometric quantities of Sn powder (99.9%, Aldrich) and Se or S powder (99.9%, Aldrich) were weighed out into silica glass tubes that were evacuated to 10^{-3} Torr and sealed. The mixture was heated at the reaction temperature (560 °C for 2H-$SnSe_2$ and 600 °C for 2H-SnS_2) for a week, ground with mortar and pestle, and annealed for another week. ZrS_2 was synthesized from stoichiometric quantities of Zr powder (99.9%, Johnson Matthey) and S powder (99.99%, Aldrich) sealed in an evacuated silica tube and heated at 900 °C for a week. The powder was then annealed for another week, and small quantities of ZrS_3, if present, were removed by sublimation. 2H- and 1T-TaS_2 were synthesized by incorporating the ideas of Revelli, although to attain the desired polytypic purity a modified cooling procedure was

(34) Mamedov, K. K.; Kerimav, I. G.; Konstryukov, V. N.; Guseinov, G. D. *Russ. J. Phys. Chem.* **1967**, *41*, 691.
(35) Mckelvy, M.; Sidorov, M.; Marie, A.; Sharma, R.; Glaunsinger, W. *Chem. Mater.* **1995**, *7*, 1045−1046.
(36) Mckelvy, M.; Sidorov, M.; Marie, A.; Sharma, R.; Glaunsinger, W. *Chem. Mater.* **1994**, *6*, 2233−2245.
(37) Mckelvy, M. J.; Sharma, R.; Glaunsinger, W. S. *Solid State Ionics* **1993**, *63*−*5*, 369−377.
(38) Barnes, P. *Phase Transitions* **1992**, *39*, 1−2.
(39) Hausermann, D.; Barnes, P. *Phase Transitions* **1992**, *39*, 99−115.
(40) Barnes, P.; Clark, S. M.; Hausermann, D.; Henderson, E.; Fentiman, C. H.; Muhamad, M. N.; Rashid, S. *Phase Transitions* **1992**, *39*, 117−128.
(41) Sheridan, A. K.; Anwar, J. *Chem. Mater.* **1996**, *8*, 1042−1051.
(42) Clark, S. M.; Irvin, P.; Flaherty, J.; Rathbone, T.; Wong, H. V.; Evans, J. S. O.; O'Hare, D. *Rev. Sci. Instrum.* **1994**, *65*, 2210.
(43) Wong, H. V.; Evans, J. S. O.; Clark, S. M.; O'Hare, D. *J. Chem. Soc., Chem. Commun.* **1994**, 809.
(44) Al-Alamy, F. A. S.; Balchin, A. A. *J. Cryst. Growth* **1977**, *38*, 221.

adopted. $TaCl_5$ (25.0 g) (Aldrich, 99.9%) was purified by vacuum sublimation at 10^{-2} Torr and 140 °C. A 12.0 g sample was loaded into an alumina boat and warmed to 200 °C over 90 min under a constant stream of H_2S (approximately one bubble per second). Excess H_2S was scrubbed by a combination of bleach and $KMnO_4/H^+$ bubblers. Sulfur was observed to form on the cold regions of the silica tube from around 160 °C. The furnace was maintained at 200 °C for 2 h, and then warmed to 900 °C for a further 3 h. The resulting black powder was heated to 200 °C under vacuum to remove any volatile impurities, then sieved to <90 μm under an inert atmosphere and annealed at 900 °C for 24 h in an evacuated quartz ampule. This procedure gave the 1T polytype. The 2H polytype was produced by slow annealing of the 1T phase. Sieved samples were sealed in a 30 cm × 1.5 cm i.d. silica ampule and placed in a tube furnace such that the load end could be maintained at a known temperature, and the empty end at room temperature, thus allowing the sublimation of excess sulfur. Attempts to use the annealing procedure of Revelli et al. failed to produce a pure 2H phase.[45] A much slower cooling cycle was adopted in which the temperature was reduced from 850 °C to 200 °C over 16 days. The polytypic purity of the resultant phase was confirmed by powder diffraction. All the powders were then sieved to the required particle size distribution. The powder X-ray diffraction patterns of the hosts corresponded closely with those available from the ICDD-PDF database [SnS_2 23-0677; $SnSe_2$ 38-1055; TiS_2 36-1406; ZrS_2 11-0679].

Cobaltocene {$Co(Cp)_2$; Cp = η-C_5H_5} was synthesized with use of a modification of the original procedure[46] by reaction of sodium cyclopentadienyl with anhydrous bis(acetylacetonate)cobalt(II) (99%, Janssen Chimica). The $Co(Cp)_2$ was purified by sublimation before use. Dimethoxyethane was predried over anhydrous 5 Å zeolite molecular sieves, distilled under an atmosphere of nitrogen, stored under N_2 in greaseless Teflon-stoppered ampules containing activated zeolite molecular sieves, and thoroughly degassed before use.

Diffraction Experiments. In situ diffraction studies were performed with use of the energy dispersive powder diffraction method on either Station 9.7 or Station 16.4 of the UK Synchrotron Radiation Source (SRS) at the Daresbury Laboratory, UK. The SRS is a low emittance storage ring that runs with an electron beam energy of 2 GeV. Stations 9.7 and 16.4 receive X-ray flux in the range 5 keV (2.5 Å) to 140 keV (0.09 Å), with a maximum intensity at about 20 keV. The position of the maximum intensity at the detector is, however, shifted to higher energy on introduction of the experimental apparatus, due to the absorption of lower energy photons by the cell materials. Useful intensity could be obtained above about 20 keV by using Pyrex glassware with a peak flux of approximately 7×10^{11} photons s^{-1} mm^2 in a 0.1% bandwidth at 10 keV. The radiation from the synchrotron passed through a collimator on to the sample, and diffracted X-rays passed through a set of post sample slits and into the detector. The detector is an intrinsic germanium crystal that counts the number of incident photons that enter it and determines their energy. The detector momentum resolution $\Delta E/E = 0.0253$ is increased by the post sample slits to $\Delta E/E = 0.0115$. A more detailed technical description of the apparatus used in these experiments has been given elsewhere.[47,48] The precise form of the energy profile $I(E_i)$ is complex and varies from reaction to reaction. The broad background observed in the Energy Dispersive X-ray Diffraction (EDXRD) spectra is due to diffuse scatter from the cell materials, sample, and solvent.

Two cell designs (Figure 2) were employed depending of the rate of the reaction being studied. Figure 2 shows a schematic diagram of the experimental setup used for measuring fast intercalation reaction where the half-lives are typically shorter than ca. 30 min. The temperature for each experiment was accurate and stable to ±1 °C.

In a typical kinetic experiment involving fast intercalation reactions microcrystalline samples of the metal dichalcogenides hosts (ca. 200−300 mg) were loaded into the flat-bottomed Pyrex flasks which were inserted into the center of the diffractometer cell. A solution of cobaltocene would then be injected into the reaction vessel via a remotely triggered solenoid valve, and accurate volumes were dispensed by precalibrating the aliquots delivered as a function of both the delivery time and nitrogen overpressure in the reservoir. To achieve isothermal conditions, solutions were preheated in the reagent reservoir before injection into the reaction vessel. Stirring was commenced a few seconds before data acquisition.

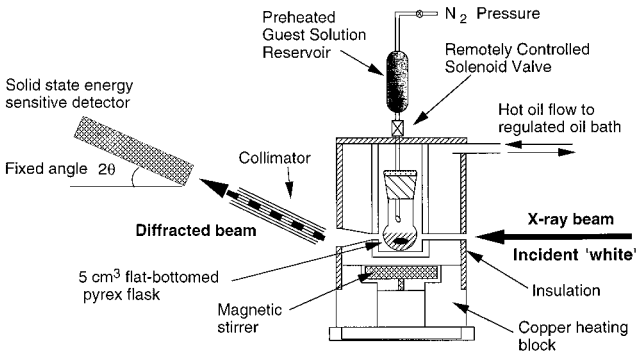

Figure 2. Schematic diagram of the in situ reaction cell used to record time-resolved energy dispersive powder X-ray diffraction data for fast intercalation reactions. For slower reactions the round-bottomed flask can be replaced with a sealed Pyrex ampule.

When reactions with much longer half-lives are studied the experimental design can be much simpler. The round-bottomed flask and injection system of Figure 2 were replaced by a flat-bottomed Pyrex ampule. Reagents were loaded in ampules and sealed with a greaseless Teflon stopcock under nitrogen in an inert atmosphere drybox. The ampule was then quickly transferred to the cell and stirring/heating was started.

Data Collection and Analysis. A typical energy-dispersive X-ray powder diffraction (EDXRD) spectrum is shown in Figure 4 for a 200 mg sample of 2H-SnS_2 suspended in 5 cm^{-3} of toluene. The total acquisition time for the spectrum shown in Figure 3 was 30 s.

The energy [E (keV)] at which a Bragg peak corresponding to a particular interplanar spacing [d (Å)] occurs in the EDXRD spectrum is given by eq 1

$$E = \frac{6.19926}{(d \sin \theta)} \qquad (1)$$

where θ is the diffraction angle in degrees (Figure 2). Thus the line at ca. 42 keV is the (001) Bragg reflection of 2H-SnS_2 (d = 5.9 Å). Since we are using white radiation atomic resonances are also excited. The peaks at 15.2 and 28.4 keV are the Sn Kα and Sn Kβ resonances, respectively.

For our experiments we chose a fixed diffraction angle (typically 2.85°) so that the (001) Bragg reflection of the intercalates (ca. 11.2 Å) occurred at ca. 22.2 keV, close to the maximum in the transmission spectrum of these samples. This geometrical setting allows the detector to sample a useable energy range equivalent to a d spacing range of approximately 20−4 Å which allows diffraction peaks due to both reactant and product to be monitored simultaneously. Integrated intensities of all the signals in the EDXRD spectra were calculated by an automated Gaussian curve fitting routine.[49] In all cases the EDXRD spectra were normalized to resonances from the metal electron cores of the host material; for ZrS_2 (Zr Kα at 15.8 keV), 2H-SnS_2 and 2H-$SnSe_2$ (Sn Kα and Sn Kβ at 25.2 and 28.5 keV), and TaS_2 (Ta Kα at 57.6 keV). This allows us to correct for small variations in the peak intensities due to varying amounts of diffracting sample in the beam during individual spectra, and minor variations in beam intensity.

Computer Simulations. Computer simulation of the intercalation reaction kinetics was modeled by using the computer program FIASCO2.[50] The program estimates the coherent diffraction from an

(45) Revelli, J. F.; DiSalvo, F. J. *Inorg. Synth.* **1979**, *19*, 35.
(46) Wilkinson, G.; Cotton, F. A.; Birmingham, J. M. *J. Inorg. Nucl. Chem.* **1956**, *2*, 95.
(47) Clark, S. M.; Nield, A.; Rathbone, T.; Flaherty, J.; Tang, C. C.; Evans, J. S. O.; Francis, R. J.; O'Hare, D. *Nucl. Instrum. Methods Phys. Res. B* **1995**, *97*, 98−101.
(48) Clark, S. M.; Irvin, P.; Flaherty, J.; Rathbone, T.; Wong, H. V.; Evans, J. S. O.; O'Hare, D. *Rev. Sci. Instrum.* **1994**, *65*, 2210−2213.
(49) Clark, S. M. *J. Appl. Crystallogr.* **1995**, *28*, 646.
(50) Evans, J. S. O. FIASCO2, 1995.

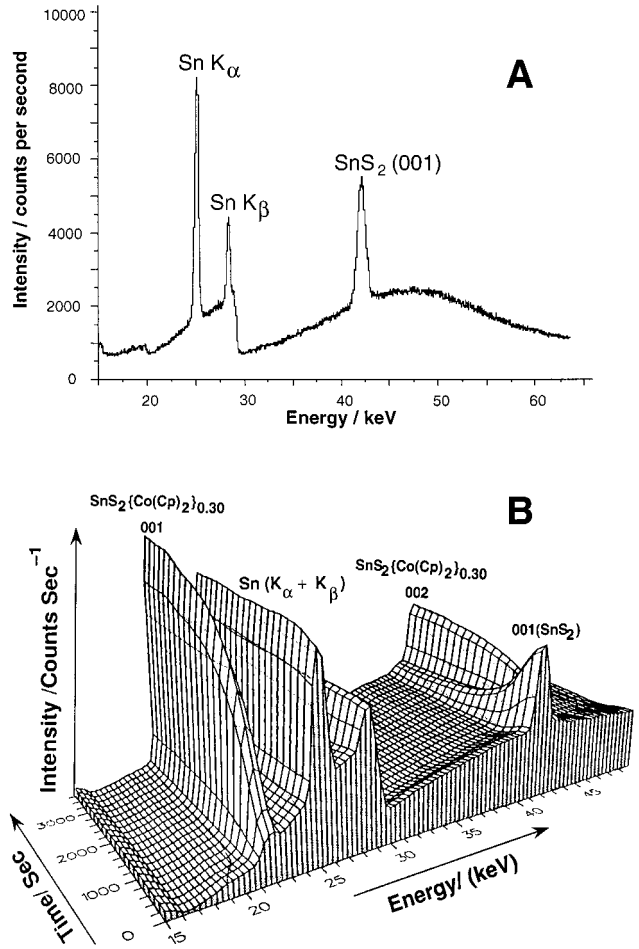

Figure 3. (a) Energy dispersive powder X-ray diffraction spectrum of a 200 mg sample of 2H-SnS_2 stirred in 5 cm^3 of toluene. Total data collection time was 30 s and the detector angle, 2θ, was 2.85°. Peak at ca. 42 keV is the (001) reflection of 2H-SnS_2. (b) Three-dimensional plot showing the energy dispersive powder X-ray diffraction spectra recorded during the intercalation of $Co(Cp)_2$ into 2H-SnS_2 at 20 °C in DME.

imaginary crystallite subdivided into $m \times n \times p$ blocks. Intercalation is simulated by a (pseudo) random process weighted by user-defined probabilities for nucleation at defect or nondefect sites followed by a user-defined 2D-diffusion rate. At each stage in the process, the amount of coherent diffraction is measured for both the host and the intercalate. In our simulations we defined coherence as having three adjacent host layers or three adjacent intercalate layers in the crystallite. The program also allows layers to enhance the intercalation of adjacent layers. A schematic representation of the basic steps in the simulation is shown in Figure 1b.

Results and Discussion

Introduction. A wide range of redox active organometallic compounds can be intercalated into the metal dichalcogenides by either direct reaction, ion-exchange, or electrochemical routes.[51] This significant reaction was first reported in 1975 when Dines described the intercalation of the metallocenes cobaltocene and chromocene into a range of metal disulfides (MS_2: M = Ti, Zr, Nb, Ta, and Sn).[15,52] Since then these materials have been extensively studied owing to their interesting structural and electronic properties. In general, the ability of an organometallic molecule to intercalate in layered lattices has always been based on ad hoc rules, and/or by trial and error. Therefore we were intrigued at the possibility of being able to quantitatively determine the kinetics of these reactions using in situ XRD techniques. This approach would also offer us the potential to identify crystalline intermediates which may be formed during the course of these reactions.

Injection of a preheated DME solution of cobaltocene {$Co(Cp)_2$; Cp = η-C_5H_5} into a suspension of 2H-SnS_2 in DME at room temperature leads to rapid intercalation of $Co(Cp)_2$ between the dichalcogenide layers giving $SnS_2\{Co(Cp)_2\}_{0.3}$. This is a first stage intercalation compound, with the *c*-axis lattice parameter increasing from 5.9 to 11.2 Å. We have previously studied the structure of this molecular intercalation compound using X-ray and neutron powder diffraction and solid state ^2H NMR and have shown that the metallocene guests are well ordered between the chalcogenide layers, with their molecular C_5-axes parallel to the layers.[53−55]

Using the in situ reactor (Figure 2), we have recorded time-resolved energy-dispersive X-ray powder diffraction (EDXRD) spectra during this intercalation reaction. The data collection electronics were initialized a few seconds before an aliquot of $Co(Cp)_2$ was injected into a stirring suspension of 2H-SnS_2 crystallites in DME. Subsequent EDXRD spectra were recorded every 20 s, and are shown in Figure 3b.

The (001) and (002) Bragg reflections associated with the intercalated phase $SnS_2\{Co(Cp)_2\}_{0.3}$ are clearly visible after a few seconds. Close examination of individual spectra during the course of the reaction revealed that there was no evidence for any new reflections which could be attributed to crystalline intermediate phases. We were particularly interested in the high *d* spacing range to see if there was any evidence for higher order stage intermediates which are commonly observed in graphite intercalation reactions.

When a toluene solution was used, some evidence was obtained that the initial phase formed during intercalation has a slightly higher *d* spacing than the final product. For the reaction of 2H-SnS_2/$Co(Cp)_2$ in toluene at 120 °C an initial intercalate phase was formed with an apparent interlayer spacing of 11.5 Å. Over a 100 min period this slowly converted to a final product with a *d* spacing of 11.2 Å (identical to that observed with DME). We attribute this behavior to the formation of an initial kinetic phase that converts over a relatively short time period to the final thermodynamic product. One possibility is that in the kinetic phase the relative packing of the guest molecules and host layers is not fully ordered. When guest molecules adopt specific, ordered interlamellar positions, the final smaller *d* spacing is observed. It is also possible that solvent co-intercalation during the course of the reaction is responsible for the larger *d* spacing of the initial phase. However, solid state ^2H NMR experiments of quenched intermediate phases from laboratory reactions with deuterated toluene as a solvent provided no evidence for solvent inclusion. A seond possibility is that the phase observed initially has the interlamellar region only partially occupied by guest molecules. The electrostatic interaction between the positively charged guest molecules and the negative layers is thus lower than that in the final product phase, leading to a larger interlayer spacing. Finally, it is possible that this phenomenon is related to a

(51) Bruce, D. W.; O'Hare, D. Inorganic Intercalation Compounds. In *Inorganic Materials*; J. Wiley & Sons: Chichester, 1992.
(52) Dines, M. B.; Gamble, F. R.; Silbernagel, B. G. *Bull. Am. Phys. Soc.* **1975**, 289.
(53) Wong, H. V.; Evans, J. S. O.; Barlow, S.; Mason, S. J.; O'Hare, D. *Inorg. Chem.* **1994**, *33*, 5515−5521.
(54) Wong, H. V.; Evans, J. S. O.; Barlow, S.; O'Hare, D. *J. Chem. Soc., Chem. Commun.* **1993**, 1589−1591.
(55) Grey, C. P.; Evans, J. S. O.; O'Hare, D.; Heyes, S. J. *J. Chem. Soc., Chem. Commun.* **1991**, 1381.

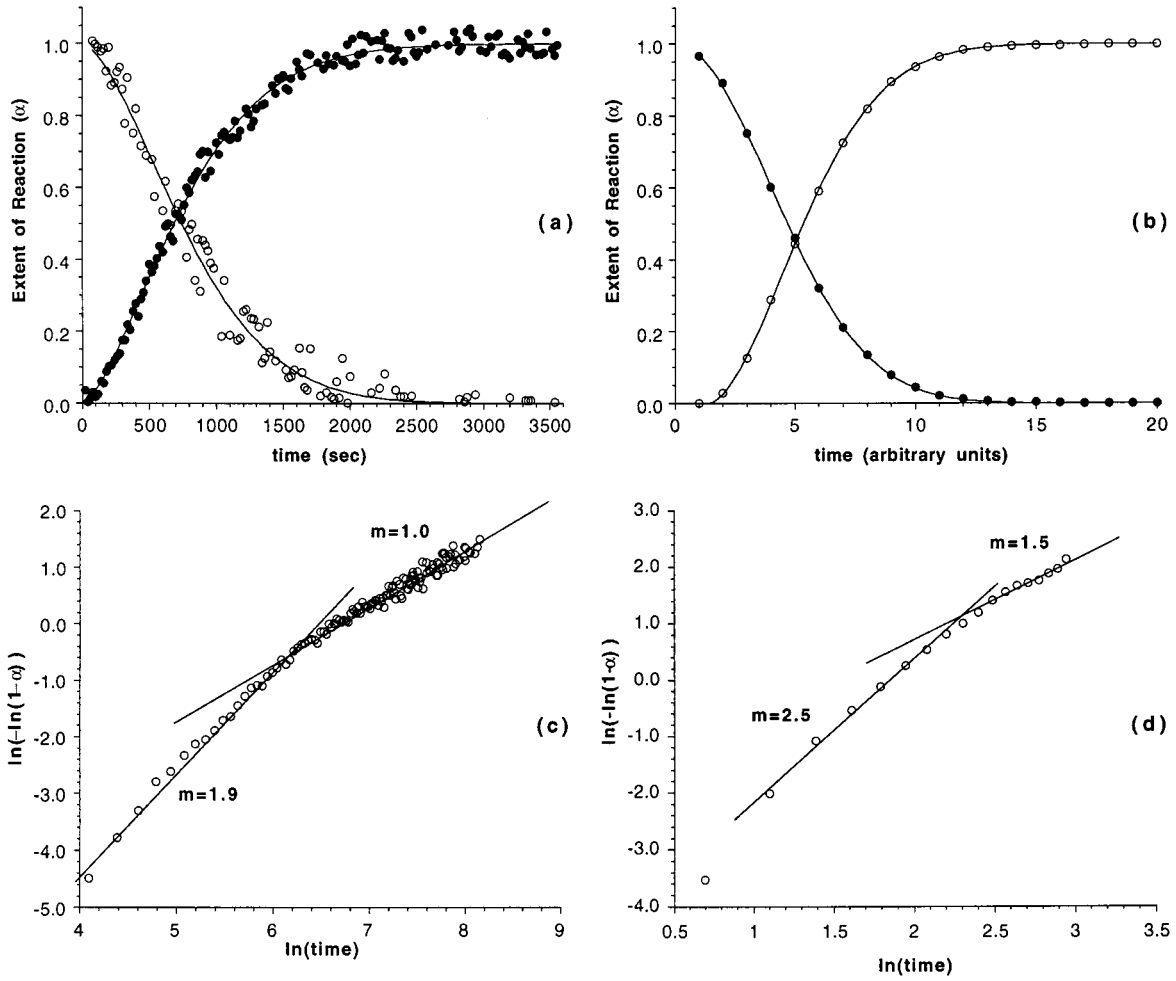

Figure 4. Kinetic data for the intercalation of $Co(Cp)_2$ by 2H-SnS_2 in DME at 20 °C: (a) Extent of reaction (α) against time (○ = 2H-SnS_2; ● = $SnS_2\{Co(C_5H_5)_2\}_{0.3}$). Solid lines are the least-squares fits to the Avrami−Erofeyev expression shown in eq 4. (b) A Fiasco statistical simulation of the reaction. (c) Sharp−Hancock plot of ln{−ln(1 − α)} vs ln(time), the gradient of the line gives the "order" of reaction *m*. (d) Sharp−Hancock plot derived from simulated data.

reorientation of the guest molecules between the layers as previously postulated for $ZrS_2/Mo(C_6H_3(CH_3)_3)$ intercalates.[56]

Given the excellent quality and signal-to-noise ratio of the EDXRD data, we were able to carry out a quantitative analysis of the data. The disappearance of the (001) reflection of 2H-SnS_2, as well as the growth of the (001) and (002) reflections of the intercalate phase, could be simultaneously monitored within our chosen spectral energy window. The integrated intensities of the host ((001); 5.9 Å) and the intercalate ((001) and (002); 11.2 and 5.6 Å) Bragg reflections were determined by Gaussian peak fitting. These integrated intensities were then normalized to the amount of diffracting sample present in the beam by dividing by the intensity of the Sn Kα resonance at 25.2 keV. To undertake a quantitative kinetic analysis of the data, it is convenient to convert the normalized experimental intensity data to the dimensionless quantity termed the extent of reaction (α). The value of α at any time (*t*) for the growth of a new crystalline phase is defined by eq 2

$$\alpha_{\text{intercalate}}(t) = \left(\frac{I_{hkl}(t)}{I_{hkl}(t_\infty)}\right) \qquad (2)$$

where $I_{hkl}(t)$ represents the integrated intensity of a reflection (*hkl*) at time *t*, and $I_{hkl}(t_\infty)$ is the integrated intensity when the reaction is complete. In addition, the decay of the host can also be followed with eq 3

$$\alpha_{\text{Host}}(t) = 1 - \left(\frac{I_{hkl}(t)}{I_{hkl}(t_0)}\right) \qquad (3)$$

where $I_{hkl}(t)$ represents the integrated intensity of a host reflection (*hkl*) at time *t*, and $I_{hkl}(t_0)$ is the initial intensity of that reflection.

Figure 4 shows the plot of the extent of reaction (α) vs time (*t*) for both the formation of $SnS_2\{Co(Cp)_2\}_{0.3}$ and the decay of 2H-SnS_2 at 20 °C. The curve is sigmoidal in shape, which is typical of many solid-state transformations in bulk powder samples.

One of the most widely used treatments of solid-state kinetics is the scheme proposed by Avrami that separates the overall course of the reaction into separate stages of product nucleation and nuclei growth and has the general functional form given by eq 4

$$\alpha(t) = 1 - \exp\{-(k_{\text{obs}}t)^m\} \qquad (4)$$

In favorable cases, the exponent *m* can be used to infer details about the rate of nucleation and the dimensionality of nuclei growth.[57] The value of *m* is perhaps most easily visualized with

(56) Evans, J. S. O.; Barlow, S.; Wong, H. V.; O'Hare, D. *Adv. Mater.* **1995**, *7*, 163−166.

(57) Hulbert, S. F. *J. Br. Ceram. Soc.* **1969**, *6*, 11.

the aid of a "Sharp−Hancock" plot, in which a plot of ln(−ln-(1 − α)) against ln(time) gives a straight line of gradient *m*.[58] It is, however, well-known that the value of *m* is extremely sensitive to the precise nature of data analysis and, in particular, to the manner in which reaction induction times are treated.

The solid lines in Figure 4a are the least-squares best fits of the α(*t*) curves for the intercalation of $Co(Cp)_2$ into 2H-SnS_2 at 20 °C to eq 4. The best fits to both the growth and decay curves give a value of the exponent, $m = 1.5$. Sharp−Hancock analysis (Figure 4c), however, suggests a more complex reaction behavior, and that the exponent *m* changes during the course of reaction with the early stages of reaction being best described by $m = 2$ and later stages by $m = 1$. This is discussed in more detail below.

Mechanism of Intercalation Reactions. Clearly the simple fitting of Avrami-type expressions to experimentally determined rate data for a process as complex as intercalation cannot lead to unambiguous mechanistic interpretation. As shown in Figure 1b, the overall process of intercalation can be broken down into several smaller steps involving nucleation of guest molecules at the edge of crystallites and subsequent diffusion of these molecules into the bulk of the host lattice; the relative rates of these two processes will determine the overall shape of the α−time curve. For a layered intercalation compound one can immediately identify two limiting cases. When the rate of diffusion of the guest molecules between individual layers is large compared to the rate of formation of new nucleation sites at the edge of the crystal, one has a situation in which the individual layers fill "instantaneously". The diffusion process one is observing when applying Avrami kinetic analysis is not then the 2D diffusion of guest molecules into the center of individual layers (as in Figure 1a), but the one-dimensional diffusion of filled layers parallel to the *c*-axis (Figure 1b).

The rate of this one-dimensional diffusion compared to the rate of nucleation of remote host layers will further effect the shapes of the α−time curves for the host and intercalate. If nucleation occurred in a completely statistical fashion within a crystallite then the loss of coherent diffraction from the host lattice would occur much more rapidly than the gain of coherent scatter from the intercalated product. If, however, the presence of guest molecules within one layer increases the probability of intercalation in adjacent layers then one would expect to observe the growth of coherent "islands" of intercalate away from initial nucleation centers (parallel to the stacking axis). In this case the growth of diffraction peaks from the intercalate and loss of host peaks would be expected to occur at comparable rates.

To investigate the influence of these various phenomena further we have developed a simple program to model the kinetics of intercalation reactions. In this program the intercalation is modeled in terms of the behavior of a hypothetical crystallite of $m \times n \times p$ blocks. The probability of a given block of the crystallite intercalating at time *t* is then influenced by a number of factors (e.g., whether it is an edge block, whether it lies within a diffusion radius distance of intercalated blocks, whether it is assigned as being a defect site, whether it is adjacent to blocks already full, its distance to a partially full layer etc.) Intercalation into a given block at time *t* is then determined in a statistical fashion, weighted by this probability. The observation of "coherent" diffraction from either host or intercalate is measured in terms of the occurrence of a specified number of adjacent intercalate/host blocks in this imaginary crystallite.

Figure 4a shows α−time curves for both the growth of intercalate and loss of host diffraction of $SnS_2/Co(Cp)_2$ in DME at 20 °C. Figure 4c shows the corresponding Sharp−Hancock plot. It is tempting to interpret the change of gradient in the Sharp−Hancock plot in terms of a change in reaction mechanism as intercalation progresses, perhaps as a shift from a nucleation controlled to a diffusion controlled process. Figure 4b shows the results of a simple statistical model of intercalation. In this simulation the rate of 2D diffusion relative to the rate of nucleation at a given layer is assumed to be infinite. Thus we consider a simple one-dimensional model of intercalation. If a given layer is intercalated then we assume that the probability of intercalation at an adjacent layer is greater than that at a random lattice site. Here adjacent $(n + 1)$ layers are assumed to be 12 times more likely to intercalate than remote layers, $(n + 2)$ layers 6 times more likely, and $(n + 3)$ layers 3 times more likely. The acceleratory rate of both intercalate and host diffraction are reproduced. Figure 4d shows a Sharp-Hancock curve derived from the simulated α−time data. Changes in gradient as a function of logarithmic time similar to those observed experimentally are observed.

Figure 5a shows α−time data for the intercalation of $Co(Cp)_2$ by 2H-$SnSe_2$ in DME at 73 °C. Figure 5b shows a simple simulation similar to that performed for 2H-SnS_2, but in which the enhancement in intercalation probability in adjacent layers is only twice that of a remote layer intercalating. Experimental and simulated Sharp−Hancock plots are shown in Figures 5c and 5d. Again an apparent change in the gradient of the Sharp−Hancock plot, from $m = 2$ to $m = 1.5$, is observed experimentally and predicted by simulation. It is also relevant to note that in the case of 2H-$SnSe_2$ the loss of diffraction from the host lattice layers occurs much more rapidly than the rate of growth of intercalate such that the α−time curves cross at $\alpha < 0.5$. On our simple one-dimensional model this would suggest that intercalation occurs in a significantly more random fashion in 2H-$SnSe_2$ than 2H-SnS_2, leading to a rapid loss of coherent diffraction from the host lattice.

Some support for this 1-dimensional model of intercalation comes from transmission electron microscopy. A small quantity of 2H-SnS_2 was stirred with a DME solution of cobaltocene for 3 min and the reaction quenched. A typical transmission electron micrograph of a crystallite with its *c*-axis perpendicular to the electron beam is shown in Figure 6. All images recorded showed distinct regions of host lattice and intercalate blocks with interlayer separations of 5.9 and 11.2 ± 0.1 Å. In all crystallites examined no evidence of staging was observed, and from the edge of the crystallite to the center, each interlayer space was completely expanded or remained nonintercalated. This is in contrast to micrographs recorded on Hg/MX_2 lattices by McKelvy and co-workers where clear and elegant evidence of staging was observed.[35−37] This technique is, of course, limited to the observation of relatively thin crystallite sections which may not be representative of the bulk.

This one-dimensional model of intercalation in which entire layers of the host lattice intercalate instantaneously may also help rationalize the relatively rare observation of staging in metallocene/MX_2 intercalates. For one to observe, for example, a second stage intercalation compound of the Daumas−Hérold type,[59] diffusing fronts of guest molecules from nearby crystal layers must meet at points in the center of a crystallite. For this to occur, the rate of formation of guest nucleation sites must be comparable to the rate of 2D diffusion of guest molecules.

(58) Hancock, J. D.; Sharp, J. H. *J. Am. Ceram. Soc.* **1972**, *55*, 74−77.

(59) Daumas, N.; Herold, A. *C. R. Acad. Sci. Paris* **1969**, *268*, 373.

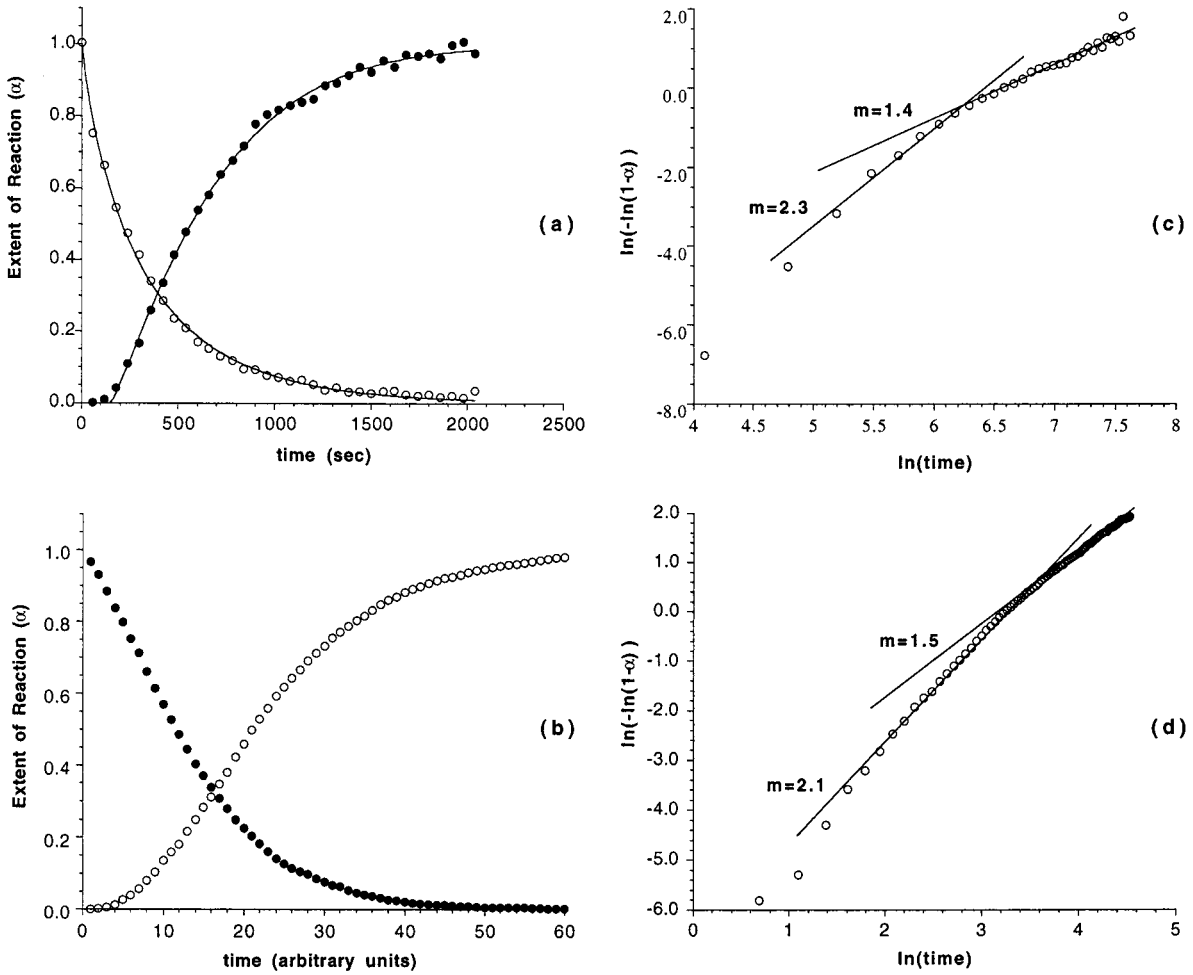

Figure 5. Kinetic data for the intercalation of $Co(Cp)_2$ by 2H-$SnSe_2$ in DME at 73 °C: (a) Extent of reaction (α) against time (○ = 2H-$SnSe_2$; ● = $SnSe_2\{Co(C_5H_5)_2\}_{0.3}$). Solid lines are the least-squares fits to the Avrami−Erofeyev expression shown in eq 4. (b) A FIASCO2 statistical simulation of the reaction. (c) Sharp−Hancock plot of $\ln\{-\ln(1-\alpha)\}$ vs ln(time), the gradient of the line gives the "order" of reaction *m*. (d) Sharp−Hancock plot derived from simulated data.

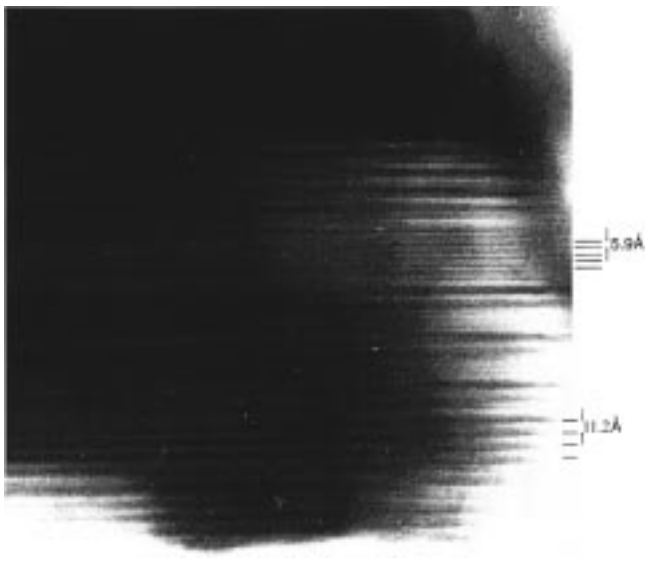

Figure 6. TEM of the partially intercalated sample $SnS_2\{Co(Cp)_2\}_{0.03}$ showing blocks of completely full and completely empty layers.

There are also polymer intercalates known, for example, poly(ethylene oxide) intercalates of $MnPS_3$,[60] where the rate of intercalation is observed to be much higher than one would expect based on a simple diffusion model of intercalation. In these cases one can envisage an extension of our 1D model in which intercalation proceeds from the surface layers of a crystallite toward its center; entire surface layers of the host lattice are coordinated by polymer, and are prised away from the bulk of the crystallite. Such a process has as its extreme a mechanism whereby the individual layers of the host lattice are flocculated prior to intercalation and restacked around guest molecules, as was initially performed in the synthesis of intercalates of MoS_2.[61]

Effect of Temperature on Intercalation. For the intercalation of 2H-SnS_2 with $Co(Cp)_2$ we have measured the temperature dependence of the reaction in the range 0−100 °C. To obtain a consistent measure of rate constants α−time data at each temperature were fitted to an Avrami expression (eq 4) with $m = 1.5$. These rate constants (Table 1) were used to construct an Arrhenius plot (Figure 7) from which we measure an apparent activation energy for the intercalation reaction of 41 ± 7 kJ mol^{-1}.

Effect of Host Lattice on the Intercalation Rate. We have also investigated the intercalation of $Co(Cp)_2$ into a range of other layered metal dichalcogenides (ZrS_2, 2H-SnS_2, 2H-$SnSe_2$, 2H-TaS_2, 2H-$NbSe_2$, 1T-TaS_2, and TiS_2). We were particularly interested in determining how the rate of $Co(Cp)_2$ intercalation

(60) Oriakhi, C. O.; Lerner, M. M. *Chem. Mater.* **1996**, *8*, 2016−2022.

(61) Divigalpitiya, W. M. R.; Frindt, R. F.; Morrison, S. R. *Science* **1989**, *246*, 369−371.

Table 1. Rate Constants for the Intercalation of $Co(Cp)_2$ by 2H−SnS_2 with DME Solvent[a]

temp (°C)	$1/T$ (10^{-3} K^{-1})	half-life (s)	k (10^{-3} s^{-1})[b]
8.5	3.552	1385(7)	0.566(3)
20	3.413	710(4)	1.100(7)
30	3.300	162(6)	4.8(2)
40	3.195	211(5)	3.71(9)
50	3.096	94(3)	8.4(3)
60	3.003	61(3)	12.9(6)
70	2.914	83(1)	9.4(1)

[a] Particle size 90−250 μm. Numbers in parentheses represent estimated error in last digit obtained by fitting eq 4 with $m = 1.5$ to the observed $\alpha(t)$ curves. When m2 was varied freely the half-life at each temperature (apart from 30 °C) varied by less than 2 standard deviations from that quoted. [b] Obtained by least-squares fitting to eq 4.

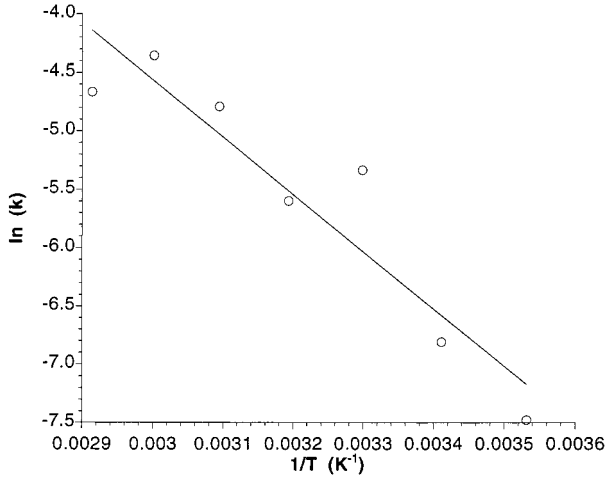

Figure 7. Plot of ln(k) vs $1/T$ for reaction of 2H-SnS_2 and $Co(Cp)_2$ in DME. All rate constants were derived by using $m = 1.5$ in eq 4.

was affected by the nature of the host lattice. In all these experiments the host lattices were sieved to obtain a uniform particle distribution in the range 60−90 μm. These reactions were all performed under standardized conditions with the same amount of stock $Co(Cp)_2$ solution at 120 °C in toluene. In each case the reaction yields a first stage intercalation compound of chemical composition $MX_2\{Co(Cp)_2\}_{0.30\pm0.05}$ (M = Zr, Sn, Ta, Ti; X = S, Se). In all cases we observed the smooth growth of intensity of the reflections of the intercalate phases with an increase in c-lattice constant of 5.35 ± 0.1 Å. No intermediate phases of higher order staging were observed in any of these reactions. $\alpha(t)$ plots for the intercalation of $Co(Cp)_2$ into ZrS_2, 2H-SnS_2, 2H-$SnSe_2$, and TaS_2 are shown in Figure 8. In each case the solid lines are the calculated least-squares fits of $\alpha(t)$ to the Avrami−Erofeyev expression given in eq 4 with an fixed value of the Avrami exponent (m) of 1.50. Time is plotted on a logarithmic scale for ease of comparison of data.

Table 2 shows a summary of the half-lives ($t_{1/2}$) and rate constants (k_{obs}/s) for the intercalation of $Co(Cp)_2$ in eight different layered metal dichalcogenide hosts. What is immediately striking about the data shown in Table 2 is the extreme variation in the rate of the reaction for each of the host lattices. Ascribing the overall rate of reaction to any one physical property of the host lattice is difficult. It might be thought that the reaction rate would be dependent on the redox properties of the host. Some feel for this redox behavior can be obtained by comparing literature discharge curves for Li/MX_2 cells. For example, the discharge potential for 2H-TaS_2 is reported to be higher than that for 1T-TaS_2, in line with the kinetic observations here. However, the discharge potential for ZrS_2 is significantly

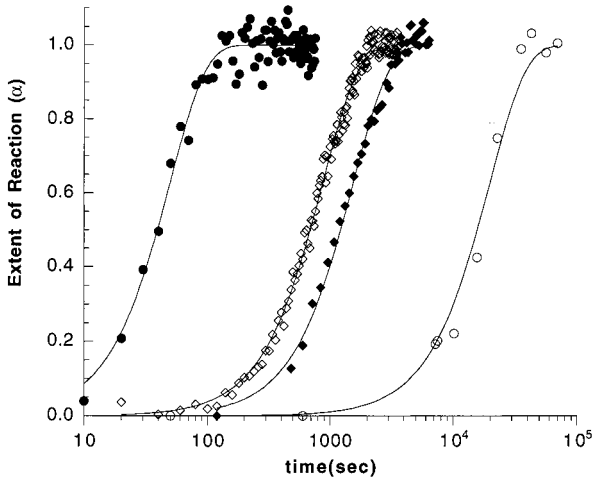

Figure 8. Extent of reaction (α) versus time for intercalation of $Co(Cp)_2$ into a range of metal dichalcogenides: ●, ZrS_2, 8 °C; ◇, 2H-SnS_2, 20 °C; ◆, 2H-$SnSe_2$, 50 °C; ○, TaS_2, 120 °C. Also shown (—) are fits to the Avrami−Erofeyev equation, $\alpha = 1 - \exp\{-(kt)\}^{1.5}$.

Table 2. The Half-Lives and Avrami Rate Constants for the Intercalation of $Co(Cp)_2$ into a Range of Lamellar Metal Dichalcogenides at 20 and 120 °C (Particle Size: 60−90 μm, in dimethoxyethane)

	20 °C		120 °C	
host	half-life (s)	10^3k ($s^{-1.5}$)	half-life (s)	10^3k ($s^{-1.5}$)
ZrS_2	23	34.1	<5	400−600[a]
2H−SnS_2	475	1.64	31	25.3
2H−SnSSe			225	
2H−$SnSe_2$	6730	0.12	410	1.92
2H−TaS_2			16000	0.05
2H−$NbSe_2$			2960	0.26
1T-TaS_2			>16000	<0.05[b]
TiS_2			>60000	<0.01

[a] At 120 °C this is too fast to measure accurately with the time resolution available; the range of values for k is an estimate based on extrapolation of lower temperature results. [b] Shortage of beam time prevented full analysis. Reaction significantly slower than that of 2H-TaS_2.

lower, yet its intercalation reactions are faster. For the intercalation of a large molecule such as cobaltocene the rate limiting factor is likely to be determined by the ease of separation of the host layers (which must increase by ca. 5.35 Å). This presumably explains the general observation that metal selenides (where van der Waals interlayer attractions are maximized) react more slowly than sulfides. It also seems likely that there is a similar explanation for the exceptionally slow rate of reaction of TiS_2. This phase shows a pronounced tendency to accommodate excess Ti in the interlamellar region ($Ti_{1+x}S_2$), which will again increase interlayer attractions.

Effects of Cobaltocene Concentration and Stoichiometry. For 2H-SnS_2, ZrS_2, and 2H-$SnSe_2$ we have also investigated the rate of intercalation as a function of the initial $Co(Cp)_2$ concentration. In each case, varying concentrations of cobaltocene solution (enough volume to provide a 2:1 molar excess with respect to the host) were injected onto 200 mg of the host lattice at a convenient temperature for kinetic analysis. Figure 9 shows each of the $\alpha(t)$ curves for the intercalation of cobaltocene into 2H-SnS_2 at 20 °C for a range of initial $Co(Cp)_2$ concentrations.

Data were fitted to the Avrami equation (eq 4) and, for the complete range of initial $Co(Cp)_2$ concentrations studied (10−70 mg cm^{-3}), the measured rate constants and half-lives were found to be invariant within experimental error (Table 3).

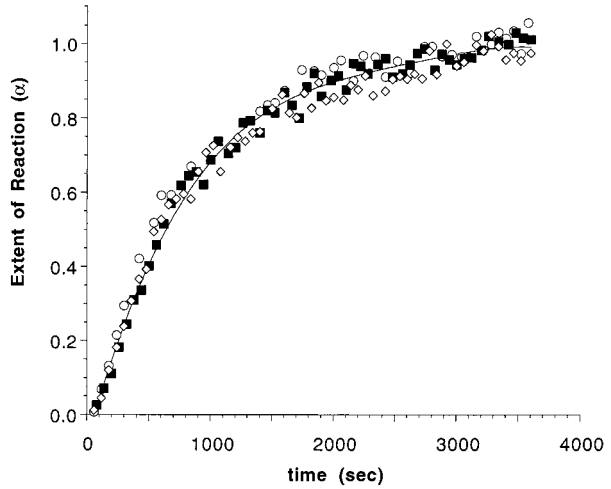

Figure 9. Extent of reaction (α) versus time for intercalation of Co(Cp)$_2$ into 2H-SnS$_2$ (particle size: 90−250 μm) with a variety of initial Co(Cp)$_2$ concentrations: ○, 12.5 mg cm^{-3}; ■, 25 mg cm^{-3}; ◆, 45 mg cm^{-3}. Reactions were performed at 20 °C for a 2:1 molar excess of guest species.

Table 3. Half-Lives for the Intercalation of Cobaltocene into Three Metal Dichalcogenides for a Range of Initial Guest Concentration[a]

	half-life (s)		
Co(Cp)$_2$ conc. (mg cm^{-3})	2H-SnS$_2$ (20 °C)	ZrS$_2$ (8°C)	2H-SnSe$_2$ (50 °C)
13	562		
26	656	36	1210
32	600	44	1160
43	640	39	1250
52	692	40	1190
64	716		

[a] Errors in half-life derived by fitting eq 4 to SnS$_2$ data are of the order of ±10 s. This probably represents an underestimate of the true error. For ZrS$_2$ the overall time of reaction is short relative to the total time required for sample injection (ca. 10 s), and errors in half-life are correspondingly large.

Therefore, we conclude that the nucleation and diffusion rate are independent of Co(Cp)$_2$ concentration over the concentration range investigated. From preliminary studies of other guest species, this phenomenon would appear to be quite general for metallocene intercalation into layered metal dichalcogenides.

If this is an example of a more general phenomena this observation has significant practical implications. The zero-order dependence in the guest concentration means that it is not necessary to use a large excess of guest molecules to expedite these reactions. This would be especially useful if the guests are expensive or particularly difficult to synthesize, or of low solubility in the solvent required.

When less than stoichiometric amounts of Co(Cp)$_2$ are added to 2H-SnS$_2$ we still see the same initial rate of reaction. Figure 10 shows the α(*t*) curve when only 0.1 equiv of Co(Cp)$_2$ are added to a 2H-SnS$_2$ suspension in toluene at 20 °C. Data have been normalized relative to the loss of the host lattice reflections. Surprisingly the α−time curve levels off at ca. 0.5 corresponding to approximately 50% conversion of the host into the final intercalate. Chemical analysis of the final product confirmed a stoichiometry of SnS$_2${Co(Cp)$_2$}$_{0.1}$. This suggests that at intermediate stages of reaction a larger than expected (ca. 50% rather than 30%) proportion of interlamellar regions have been intercalated, and that the guest molecules are, therefore, not close packed within a given host layer.

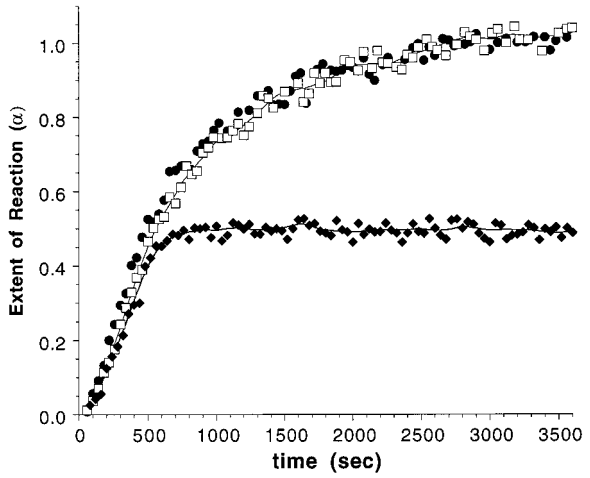

Figure 10. Extent of reaction versus time for the intercalation of Co(Cp)$_2$ into 2H-SnS$_2$ at 20 °C for a range of guest stoichiometries; the data are extracted from integration of the host (001) reflection such that α = 1 corresponds to complete loss of coherent diffraction from the host lattice. Data shown are for guest:host molar ratios of 1:1 (○), 0.33:1 (□), and 0.1:1 (◆).

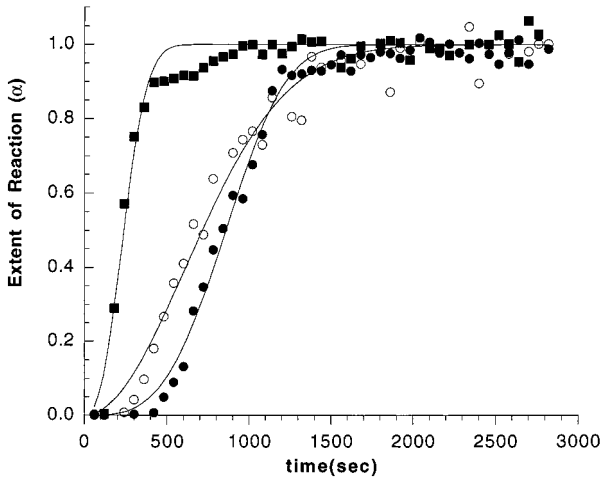

Figure 11. Extent of reaction (α) versus time for intercalation of Co(Cp)$_2$ into 2H-SnS$_2$ at 70 °C (particle size: 90−250 μm) for a range of solvents: pyridine (■), DME (○), and CH$_3$CN (●). Solid lines are fits to the Avrami−Erofeyev equation, $\alpha = 1 - \exp\{-(kt)\}^{1.5}$.

Table 4. Half-Life Values for the Intercalation of Co(Cp)$_2$ into 2H-SnSe$_2$ from Various Solvents (Dielectric Constants Obtained from the *Handbook of Chemistry and Physics* or the *Bruker Almanac*)

solvent	half-life (s)	ε(20 °C)
pyridine	250	12.4
DME	700	7.2
acetonitrile	850	37.5
THF	∼2000	7.6
benzene	>3600	2.28

Effect of Solvent on the Intercalation Rate. In situ experiments have also shown the importance of solvent on these reactions. Table 4 gives the half-life values for formation of SnSe$_2$(CoCp$_2$)$_{0.3}$ in a range of solvents at 75 °C, with the α-time data shown in Figure 11.

Intercalation is seen to be most rapid in pyridine, acetonitrile, and DME, yet substantially inhibited in benzene and THF. Similar solvent effects are observed for 2H-SnS$_2$, with DME and pyridine reactions proving quicker than those with CH$_3$CN, toluene, and benzene as solvents. The dielectric constant of benzene (2.284 at 20 °C) is significantly smaller than the

other solvents, which, given the redox nature of the intercalation process, may account for the decreased reaction rate in nonpolar solvents. However, the dielectric constant of acetonitrile (37.5 at 20 °C) is roughly three times that of pyridine (12.3 at 25 °C) yet the half-intercalation time is roughly three times longer, so other factors are almost certainly involved. In none of these reaction do we see any evidence for solvent cointercalation in the final products. We cannot rule out the possibility that transient solvent cointercalation may play an important role.

Conclusions

Time-resolved, in situ, energy dispersive powder X-ray diffraction techniques have been successfully developed to study the kinetics of intercalation of air-sensitive guests into microcrystalline host lattices. The experiment has excellent time resolution and can yield EDXRD data with good signal-to-noise on small samples (200−300 mg) with <10 s resolution.

The dependence of reaction rate on host lattice, temperature, solvent, and guest concentration has been investigated. A simple statistical model to explain the observed kinetics has been proposed.

Perhaps one of the most remarkable and significant observations is the zero dependence of the $Co(Cp)_2$ concentration on the rate of intercalation in these materials.

Acknowledgment. We would like to thank Daresbury Laboratory, UK and the EPSRC for their support and access to the Synchrotron Radiation Source, Dr. S. M. Clark of Daresbury Laboratory and the technical staff for their help in the design and construction of the experimental cell, Dr. C. J. Nuttall for assistance with data collection, and Dr. S. J. Mason for assistance with solid state NMR measurements. H.V.W. gratefully acknowledges the Rhodes Trust for a scholarship.

JA9819099